Available online at www.sciencedirect.com
ScienceDirect
Polymer 47 (2006) 8436–8443
polymer
www.elsevier.com/locate/polymer

Poly(9,9-dihexylfluorene) derivatives containing electron-transporting aromatic triazole segments: Synthesis, optical and electrochemical properties

Shinn-Horng Chen, Chuen-Shiou Shiau, Lin-Ren Tsai, Yun Chen*

Department of Chemical Engineering, National Cheng Kung University, No. 1 Da-Syue Road, Tainan 701, Taiwan

Received 31 August 2006; received in revised form 15 October 2006; accepted 25 October 2006
Available online 15 November 2006

Abstract

We prepared three new poly(9,9-dihexylfluorene) derivatives (**P1**–**P3**) containing kinked aromatic triazole (triphenyl-1,2,4-triazole derivative) via Suzuki coupling polymerization. These copolymers were soluble in common organic solvents and showed high decomposition temperatures ($T_d = 416$–454 °C). The optical and electrochemical properties of **P1**–**P3** were compared with poly(9,9-dihexylfluorene) (**PFO**) and **P4** and **P5** in which the linkages of the aromatic triazole were different. After introducing the triazole units, absorption spectra showed blue shift (388 nm → 372 nm) due to reduced conjugation, but PL spectra remained almost unchanged (417–418 nm). The linkages of triazole with fluorene segments in **P1**–**P5** were different: (1) fluorene segments linked with triazole through a kinked angle (**P1** and **P2**), (2) triazole as a branch unit (**P3**) and as terminal groups (**P4**), (3) fluorene segments linked with triazole in a linear way (**P5**). As estimated from semi-empirical MNDO calculation, two twisted conformations (ca. 90° each) exist between triazole core and fluorene groups. These kinked conformation and twisted structure increased the PL efficiency ($\Phi_{PL} = 0.60$–0.73, $\Phi_{PL} = 0.58$ for **PFO**) and partially inhibited annealing-induced excimer formation. From cyclic voltammetric results, **P1**–**P3** exhibited better electron affinity (LUMO: −2.75 to −2.82 eV) than **PFO** (LUMO: −2.52 eV).

Keywords: Polyfluorene; Aromatic triazole; Optical and electrochemical properties

1. Introduction

Conjugated polymers contain delocalized π-electrons bonding along backbone that support the mobility of charges and possess semiconducting properties. Electroluminescence (EL) from fully conjugated polymers, main-chain polymers with isolated chromophores, side-chain polymers with linked chromophores, or polymeric blends have been the subject of recent extensive studies [1–9]. However, fully conjugated polymers actually consist of chromophores with different energy gaps because the effective conjugation length is statistically distributed due to the presence of structural defects. Thus the chromophores with lower energy gaps will be the emitting species via reabsorption or energy transfer [10,11]. Confinement of conjugation into a well-defined length of polymeric chain is one of the most successful strategies to solve this problem [12–14]. Furthermore, in previous studies we found that formation of interchain interaction can be reduced by limiting the effective conjugation length [15–17].

Polyfluorene derivatives are a particularly suitable class of EL materials because they contain a rigid biphenyl unit which leads to a large band gap with efficient blue emission, and the facile substitution at C9 position provides the possibility of improving their solubility and processability by derivation. Recently, polyfluorenes (PFs) have been introduced as a prospective emitting layer with emission wavelengths primarily in the blue spectral region. PFs are more thermally stable than PPV and display high PL efficiencies both in solution and as solid films [18–21]. Unfortunately, poly[2,7-(9,9-dialkyl fluorene)]s and poly[2,7-(9-alkyl fluorene)]s generally show some excimer emission in the solid state that affects the color emission and the life time of their EL devices.

* Corresponding author. Tel./fax: +886 6 2085843.
E-mail address: yunchen@mail.ncku.edu.tw (Y. Chen).

0032-3861/$ - see front matter © 2006 Elsevier Ltd. All rights reserved.
doi:10.1016/j.polymer.2006.10.028

Aromatic triazole is an interesting electron-injection/transport chromophore because it possesses high electron affinity and thermal stability [22,23]. Furthermore, the molecular modeling reported by Strukelj et al. suggested that the triazole unit is orthogonal to the benzene rings [24]. This twisted conformation not only relieves the steric crowding between the phenylene rings attached to the triazole but also effectively limits the conjugation. Such segmentation is a recognized strategy for improving the fluorescence quantum efficiency and blue shifting the emission, as has been reported for both saturated spacer polymers and copolymers with *meta*-phenylene conjugation-limiting units.

In this work, we prepared poly(9,9-dihexylfluorene) (**PFO**) and three poly(9,9-dihexylfluorene) derivatives (**P1**–**P3**) containing electron-transporting aromatic triazole chromophores using Suzuki coupling reaction. The oligofluorene segments were linked with a triazole core via a kinked angle, in which the triazoles were difunctional (**P2** and **P3**) or trifunctional (**P4**) moieties. Optical and electrochemical properties of these copolymers have been investigated in detail. Moreover, the kinked conformation and twisted structure between triazole core and fluorene segments are expected to reduce main-chain conjugation and suppress the formation of interchain interactions.

2. Experimental

2.1. Materials and measurements

The synthetic procedures of compounds **1**, **4**, poly(9,9-dihexylfluorene) (**PFO**), **P4** and **P5** (Scheme 2) are described in the literature elsewhere [25]. 4-Bromoaniline (**2**, Alfa Aesar), 9,9-dihexylfluorene-2,7-bis(trimethyleneborate) (**6**, Aldrich), 2,7-dibromo-9,9-dihexyl-9*H*-fluorene (**7**, Aldrich), and *N*,*N*-dimethylaniline (TCI) were pure reagents and used as received. The solvents such as chloroform ($CHCl_3$, Tedia Co.), *N*,*N*-dimethylformamide (DMF, Tedia Co.), dimethylsulfoxide (DMSO), and toluene (Tedia Co.) were HPLC grade reagents and used without purification. All new compounds were identified by ^{1}H NMR, FT-IR, and elemental analysis (EA). The ^{1}H NMR spectra were recorded on a Bruker AMX-400 MHz FT-NMR, and chemical shifts are reported in ppm using tetramethylsilane (TMS) as an internal standard. The FT-IR spectra were measured as KBr disk on a Fourier transform infrared spectrometer, model Valor III from Jasco. The elemental analysis was carried out on a Heraus CHN-Rapid elemental analyzer. The thermogravimetric analysis (TGA) of the polymers was performed under nitrogen atmosphere at a heating rate of 20 °C/min using a Perkin–Elmer TGA-7 thermal analyzer. Thermal properties of the polymers were carried out using a differential scanning calorimeter (DSC), Perkin–Elmer DSC 7, under nitrogen atmosphere at a heating rate of 20 °C/min. UV–vis absorption spectra were measured with a Jasco V-550 spectrophotometer. The steady-state photoluminescence (PL) spectra were recorded on Hitachi F-4500 fluorescence spectrophotometer. The cyclic voltammograms were recorded using a voltammetric analyzer, model CV-50W from BAS, under nitrogen atmosphere using ITO glass as working electrode, Ag/AgCl electrode as reference electrode and platinum wire electrode as auxiliary electrode immersed in 0.1 M $(n\text{-Bu})_4NClO_4$ in acetonitrile. The energy levels were calculated using the ferrocene (FOC) value of −4.8 eV with respect to vacuum level, which is defined as zero [26].

2.2. Monomer synthesis (Scheme 1)

2.2.1. 3,4-Bis(4-bromophenyl)-5-(4-fluoro-3-(trifluoromethyl)phenyl)-4H-1,2,4-triazole (3)

To a two-necked 25-mL glass reactor was charged compound **1** (0.89 g, 2 mmol), 4-bromoaniline (**2**: 0.34 g, 2 mmol), and 10 mL *N*,*N*-dimethylaniline. The reaction mixture was stirred at 135 °C for 24 h in nitrogen atmosphere and poured into 2 N $HCl_{(aq)}$ after cooling. The precipitate was collected by filtration and recrystallized from ethyl acetate/dichloromethane. It was further purified by column chromatography using ethyl acetate/dichloromethane (v/v = 6/4) as eluent. Evaporation of the eluent afforded yellow solid of **3** (47.6%) (Scheme 1). Mp = 218–219 °C. ^{1}H NMR (acetone-d_6, ppm): δ 7.90–7.87 (d, 2H, ArH), 7.80–7.77 (d, 2H, ArH), 7.68–7.60 (m, 4H, ArH), 7.56–7.50 (m, 3H, ArH). FT-IR (KBr pellet, cm^{-1}): ν 1134, 1160, 1241, 1316 (C–F), 1055 (C–Br), 1622 (N–H). Anal. Calcd. (%) for $C_{21}H_{11}Br_2F_4N_3$: C, 46.61; H, 2.05; N, 7.77. Found: C, 46.40; H, 2.10; N, 7.77.

2.2.2. 3,4,5-Tris(4-bromophenyl)-4H-1,2,4-triazole (5)

To a two-necked 25-mL glass reactor was charged **4** (0.30 g, 0.6 mmol), **2** (0.10 g, 0.6 mmol), and 3 mL *N*,*N*-dimethylaniline. The reaction mixture was heated to 135 °C under nitrogen atmosphere and stirred for 24 h. After the reaction was completed, the mixture was poured into 2 N $HCl_{(aq)}$ and the precipitates were collected by filtration. The crude products were recrystallized from ethyl acetate/dichloromethane and further purified by column chromatography using ethyl acetate/dichloromethane (v/v = 6/4) as eluent. Evaporation of the eluent afforded yellow solid of **5** (20.2%). Mp: above 250 °C. ^{1}H NMR (acetone-d_6, ppm): δ 7.70–7.66 (d, 2H, ArH), 7.63–7.59 (d, 4H, ArH), 7.41–7.37 (d, 2H, ArH), 7.33–7.30 (d, 4H, ArH). FT-IR (KBr pellet, cm^{-1}): ν 1074 (C–Br), 1594 (N–H). Anal. Calcd. (%) for $C_{20}H_{12}Br_3N_3$: N, 7.87; C, 44.98; H, 2.26. Found: N, 7.68; C, 44.59; H, 2.21.

2.3. Synthesis of polymers (Scheme 1)

The polymers were synthesized via the palladium-catalyzed Suzuki coupling reaction. A general procedure for the polymerization is as follows: to 4.5 mL toluene were added diborate (**6**), dibromofluorene (**7**), triazole monomers (**3** or **5**), and 2 M aqueous solution of Na_2CO_3 (1 mL). The mixture was vigorously stirred at 90 °C for 20 h after adding the catalyst $Pd(PPh_3)_4$ (0.0058 g). Finally, the terminal reactive groups were end-capped with suitable capping agents. For example, **P1** was prepared from **6** (0.276 g, 0.55 mmol), **7** (0.246 g, 0.5 mmol) and **3** (0.027 g, 0.05 mmol) via the palladium-catalyzed Suzuki coupling reaction. After the reaction it was

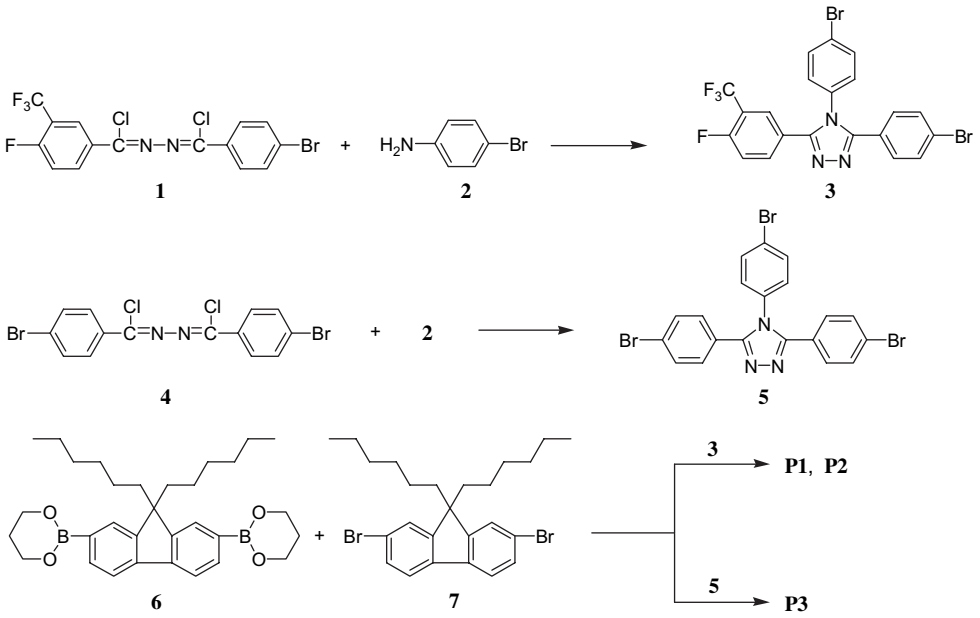

Scheme 1.

successively end-capped with phenylboric acid and bromobenzene for 6 h each, then precipitated from methanol/de-ionized water (v/v = 10/1). The precipitates were collected by filtration and further purified by extracting with acetone for 24 h using a Soxhlet extractor. **P2** was prepared by the same procedures except the content of aromatic triazole monomer was increased (**6**: 0.254 g, 0.5 mmol; **7**: 0.197 g, 0.4 mmol; **3**: 0.054 g, 0.1 mmol). Similar procedures were employed to synthesize **P3** except that trifunctional compound **5** was used as aromatic triazole monomer instead of difunctional monomer **3**, with the mole feed of **6**:**7**:**5** = 0.5:0.5:0.033.

P1: ^{1}H NMR ($CDCl_3$, ppm): δ 7.82 (d, 2H, ArH), 7.67–7.61 (m, 16H, ArH), 2.29–2.12 (s, 4H, $-CH_2-$), 1.14 (s, 8H, $-CH_2-$), 0.79 (s, 3H, $-CH_3$). FT-IR (KBr pellet, cm^{-1}): ν 1140, 1249, 1316 (C–F), 1055 (C–Br). Anal. Calcd. (%): C, 89.05; H, 9.35; N, 0.57. Found: C, 86.5; H, 9.17; N, 0.63.

P2: ^{1}H NMR ($CDCl_3$, ppm): δ 7.81–7.70 (d, 2H, ArH), 7.66–7.44 (d, 16H, ArH), 2.09–2.08 (s, 4H, $-CH_2-$), 1.24–1.12 (s, 16H, $-CH_2-$), 0.78 (s, 6H, $-CH_3$). FT-IR (KBr pellet, cm^{-1}): ν 1140, 1241, 1316 (C–F), 1055 (C–Br), 1622 (N–H). Anal. Calcd. (%): C, 87.57; H, 8.93; N, 1.25. Found: C, 86.8; H, 9.01; N, 1.14.

P3: ^{1}H NMR ($CDCl_3$, ppm): δ 7.98–7.95 (d, 2H, ArH), 7.86–7.66 (d, 16H, ArH), 2.13–2.10 (s, 4H, $-CH_2-$), 1.12–0.78 (d, 16H, $-CH_2-$), 0.78–0.56 (m, 6H, $-CH_3$). FT-IR (KBr pellet, cm^{-1}): ν 1055 (C–Br), 1594 (N–H). Anal. Calcd. (%): C, 90.05; H, 9.54; N, 0.41. Found: C, 84.74; H, 8.9; N, 0.58.

3. Results and discussion

3.1. Synthesis and characterization

The preparation of polymers **P1**–**P3** was based on palladium-catalyzed Suzuki coupling reaction, which was carried out in a mixture of toluene and aqueous Na_2CO_3 solution under vigorous stirring. The contents of the aromatic triazole chromophores in **P1**–**P3** were 5.2, 9.84, and 5.7 mol%, respectively, estimated from elemental analytical data. The molecular weights, molecular weight distributions, and thermal decomposition temperatures of **P1**–**P3** are summarized in Table 1. The copolymers are soluble in common organic solvents such as chloroform, THF and 1,1,2,2-tetrachloroethane. The weight-average molecular weights (M_w) of **P1**–**P3**, determined by gel permeation chromatography against polystyrene as standard, were 1.17×10^4, 2.95×10^4, and 6.0×10^3, respectively, with polydispersity indexes lying between 1.49 and 1.51. The lower molecular weight of **P3** is probably due to mole ratio difference between diborate monomer (**6**) and bromide monomers (**7** and **5**). But the polymerization led to gel in short time (ca. 20 min) if the mole ratio was 1:1. Thermal stability of the polymers was evaluated by thermogravimetric analysis (TGA) under nitrogen atmosphere and their thermograms are depicted in Fig. 1. The thermal decomposition temperatures (T_d) of **P1**–**P3** are 416, 454, and 425 °C, respectively. No melting temperature and obvious T_g (the glass transition temperature) could be observed below 300 °C on their DSC thermograms. The results suggest that the copolymers are basically amorphous materials with good thermal stability.

3.2. Optical properties

Fig. 2 illustrates the absorption and photoluminescence (PL) spectra of **PFO** and copolymers **P1**–**P3** with their optical data summarized in Table 2. The absorption maxima of **PFO**, **P1**–**P3** in $CHCl_3$ locate at 388, 384, 379, and 372 nm, and the emission peaks appear at 418, 418, 417, and 417 nm, respectively. Clearly, the absorption peaks show hypsochromic shift after introducing triazole segments, suggesting that the aromatic triazole segments interrupt the linear π-system of

Table 1
Characterization and solubility of **P1**–**P5**[a]

No.	M_w[b] ($\times 10^4$)	PDI[b]	T_d[c] (°C)	Solubility[d]						
				DMF	DMSO	NMP	$CHCl_3$	$C_2H_2Cl_4$	THF	TL
P1	1.17	1.51	416	+	+−	+	++	++	++	++
P2	2.95	1.49	454	+−	−−	++	++	++	++	++
P3	0.60	1.50	425	+−	−−	+−	++	++	++	+
P4[e]	3.08	2.14	439	+	+−	+−	++	+	++	+−
P5[e]	14.6	3.47	458	+−	−−	++	++	++	++	++

[a] Polymerized at 90 °C for 20 h.
[b] M_n, M_w, and PDI of the polymers were determined by gel permeation chromatography using polystyrene standards in $CHCl_3$.
[c] The temperature at 5% weight loss.
[d] ++: soluble at room temperature, +: soluble by heating, +−: partially soluble and/or swelling, −−: insoluble.
[e] The data are cited from Ref. [25].

polyfluorene that leads to conjugation confinement. The optimized molecular geometries of segment between triazole linked with fluorene chromophores in **P1** and **P3** were obtained by minimizing energy via semi-empirical MNDO calculations in gas state [27]. The twist angles between adjacent aromatic rings while going from fluorene to triazole core are about 90°, confirming that incorporation of aromatic triazole chromophores into polyfluorene diminishes its effective conjugation length. However, the PL emission peaks of **P1**–**P3** in $CHCl_3$ (417–418 nm) are almost the same as **PFO** (418 nm) which is a blue-emitting material. However, the emissions originating from aromatic triazole segments were not observed. The PL spectrum of monomer **5** exhibits a peak at 352 nm, which overlaps greatly with the absorption spectra (λ_{max} at 388 nm) of polyfluorene. This result suggests that the energy might transfer from triazole segments to oligofluorene segments in **P1**–**P3**. Therefore, the emission at 417–418 nm of **P1**–**P3** is possibly owing to efficient energy transfer from aromatic triazole chromophores to oligofluorene segments whose emission maxima are at around 418 nm. Therefore, polyfluorene can be modified by aromatic triazole chromophores without a large shifting in its emission spectra. Furthermore, the copolymers **P1**–**P3** show higher PL efficiency ($\Phi_{PL} = 0.60$–0.73) than that of **PFO** ($\Phi_{PL} = 0.58$). This is simply owing to increased confinement of the conjugation in backbone after incorporating triazole segments, which effectively prevent the trapping of excitons by defects or reduce the interchain interaction [15–17].

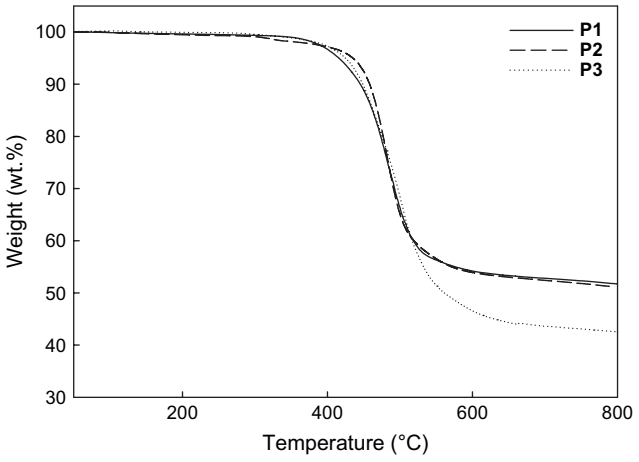

Fig. 1. The thermogravimetric analysis of **P1**–**P3** under nitrogen atmosphere at a heating rate of 20 °C/min.

The absorption and emission spectra of **P1**–**P3** in the film state both reveal red shift as compared to those in solution (Table 2), suggesting the formation of interchain interaction during film casting process. The PL spectral red shifts of **P1**–**P3** are in the range of 4–7 nm, similar to the absorption red shift (2–9 nm). Therefore, the red shifts can be attributed to the aggregate formation in solid state. In order to study optical stability of the copolymers upon heating we investigated the variations in their absorption and emission spectra during thermal annealing. The films of **P1**–**P3** were first annealed at 100, 150, and 200 °C for 1 h, respectively, to investigate heat-induced absorption and PL spectral changes. As shown in Fig. 3, no obvious absorption red shift occurs after the annealing process. However, a new broad band appears at around 522 nm in PL spectra after the annealing process and its intensity enhances gradually with increased annealing temperatures (Fig. 4). Therefore, it is reasonable to infer that the new emission (522 nm) is mainly owing to excimer formation [17]. Bliznyuk et al. suggested that the excimer-induced peak at around 522 nm is the result of excitation energy delocalization among three neighboring polymeric chains. As shown in Fig. 5, the PL spectra of **PFO**, **P4** (3.8 mol% triazole), and **P5** (10.3 mol% triazole, Scheme 2) exhibit the excimer emission after thermal annealing as well. However, the intensity of **PFO** at 524 nm is much higher than those of **P1**–**P5** at 512–523 nm. This clearly reveals that the aromatic triazole segments are effective in suppressing the excimer formation, especially the branching triazole in **P3** which shows the least intensity in the excimer emission. Previous studies on polyfluorene suggested that the green emission was also possibly attributable to the formation of ketone defects in C9 position of fluorene unit [28,29]. However, no absorption at around 1718 cm^{-1} (the ketone absorption) was detected in IR spectra of **P1**–**P3** after the annealing treatment, suggesting that the ketone effect can be excluded from these copolymers containing aromatic triazole moieties.

In a previous study on energy transfer, we found that protonation of energy donors might lead to incomplete energy transfer depending on the degree of protonation [30].

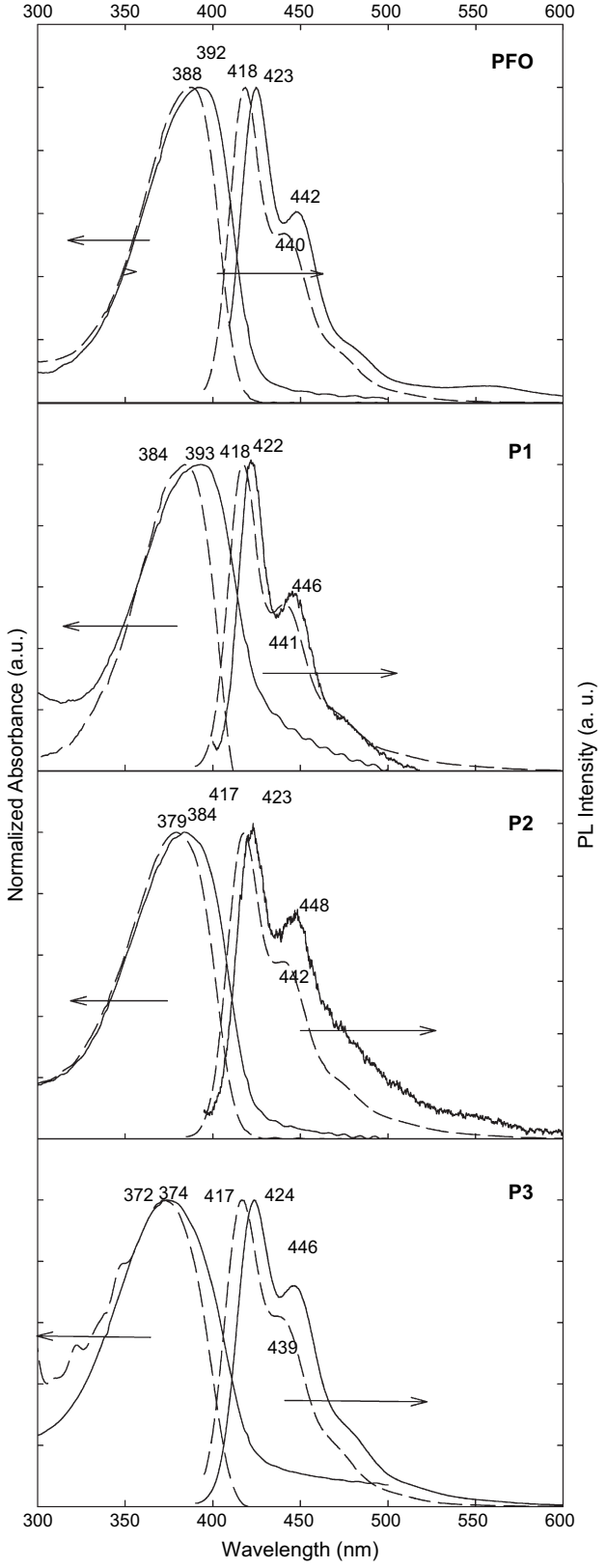

Fig. 2. PL and absorption spectra of **PFO** and **P1**–**P3** in $CHCl_3$ (- - -: 10^{-5} M) and as films (—).

Accordingly, protonation of energy donors (aromatic triazole) in **P1**–**P3** can also be observed similarly and employed to find out the emission wavelength of the triazole chromophores.

Table 2
Optical Properties of **PFO** and **P1**–**P5**

No.	UV–vis λ_{max}[a] (solution, nm)	UV–vis λ_{max} (film, nm)	PL λ_{max} (solution, nm)	PL λ_{max} (film, nm)	Φ_{PL}[b]
PFO	388	392	418, 440, 476s	423, 442, 483s	0.58
P1	384	393	418, 441, 478s	422, 446	0.64
P2	379	384	417, 442, 478s	423, 448	0.73
P3	372	374	417, 439, 477s	424, 446, 482s	0.60
P4[c]	384	390	418, 440, 478s	424, 448, 483s	0.46
P5[c]	381	389	417, 441, 476s	422, 447, 484s	0.64

[a] 1×10^{-5} M in $CHCl_3$.
[b] These values were estimated by using quinine sulfate (dissolved in 1 N $H_2SO_{4(aq)}$ with a concentration of 10^{-5} M, assuming $\Phi_{PL} = 0.55$) as a standard.
[c] The data are cited from Ref. [25].

Fig. 6 illustrates the PL spectra of **P1**–**P3** in acetic acid and chloroform. Comparing the emission spectra of **P1**–**P3** in $CHCl_3$, the PL spectra in acetic acid are broadened and exhibit

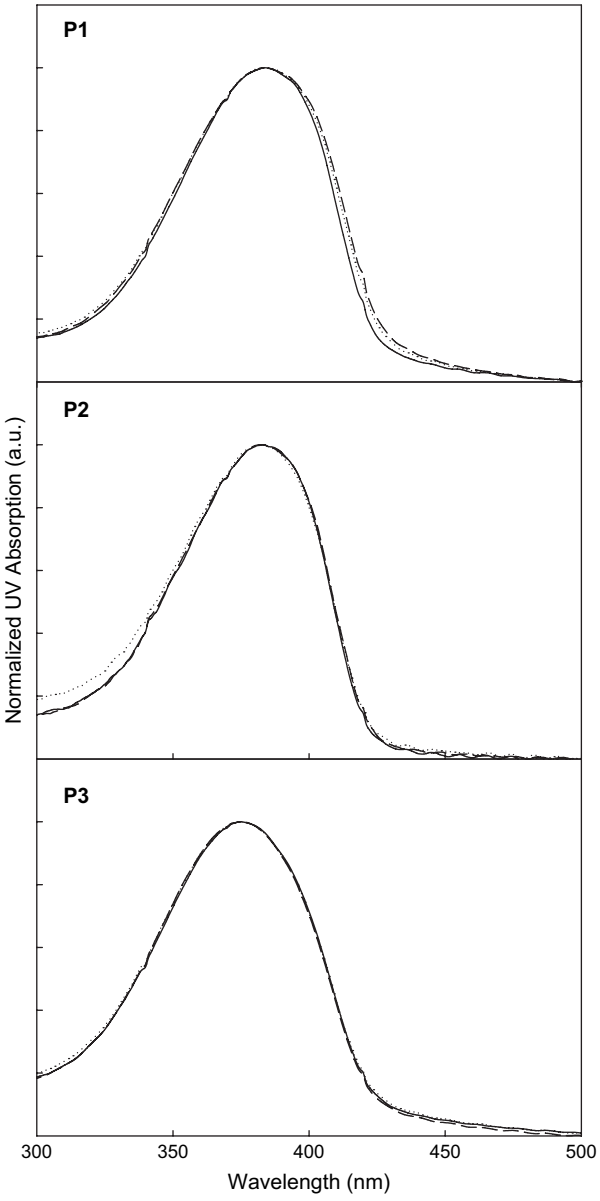

Fig. 3. Absorption spectra of **P1**–**P3** after thermal annealing for 1 h [(—) at 100, (—) 150, and (···) 200 °C].

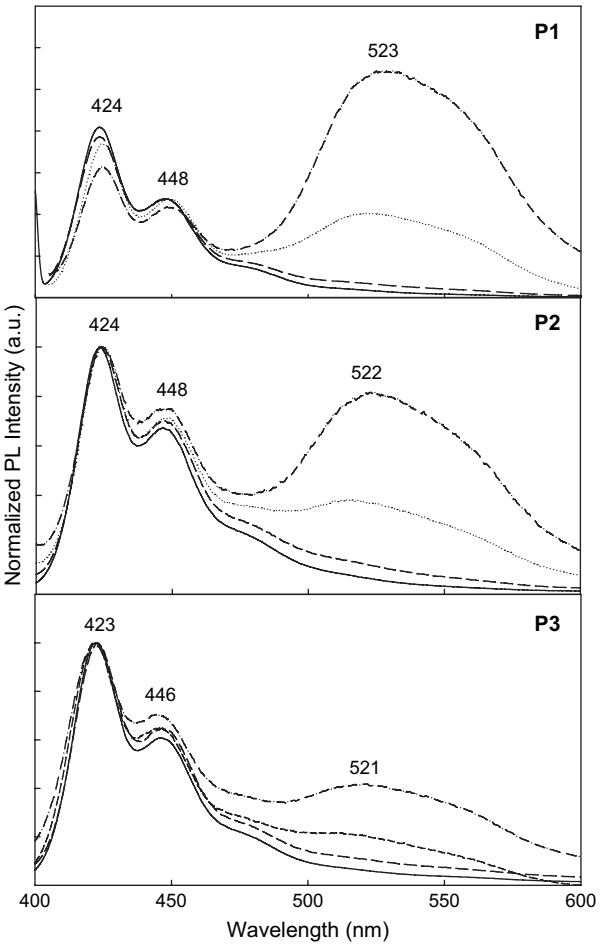

Fig. 4. PL spectra of **P1**–**P3** films after thermal annealing for 1 h [(—) pristine films, (—) at 100, (···) 150, and (-·-·-) 200 °C].

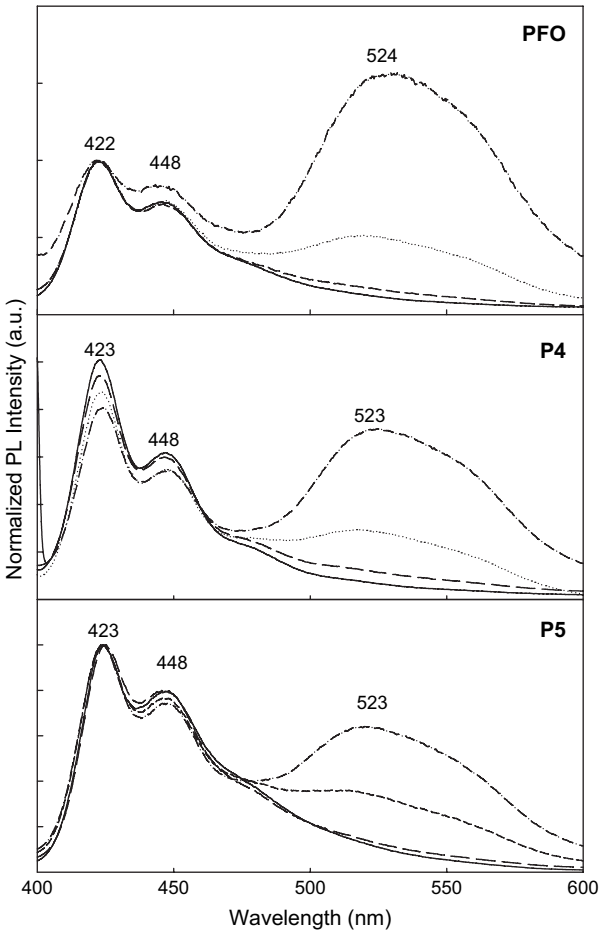

Fig. 5. PL spectra of **PFO**, **P4**, and **P5** films after thermal annealing for 1 h [(—) pristine film, (—) at 100, (···) 150, and (-·-·-) 200 °C].

slight red shift when excited with the absorption maxima of the polymers (Excitation 384 nm). Accordingly, protonation of the energy donor (triazole: electron acceptor) stabilizes excited state more than the ground state leading to red shift in emission. Monkman et al. also demonstrated that the protonation of nitrogen had an important structural effect and led to red shifts of both absorption and emission spectra [31]. When **P1**–**P3** in the acetic solution were excited with maximum absorption of energy donors (266 nm), they exhibit a new peak at around 320 nm which is contributable to energy donors under acidic condition. Protonation of triazole units strongly affects the σ-bond network, but it merely serves to electrostatically lower the energy of π-orbital. This in turn will lower the probability of energy transfer from the triazole groups to the fluorene segments. Therefore, the PL of the triazole groups is obviously observed at 320 nm when they are protonated, but not when they are unprotonated.

3.3. Electrochemical properties

We employed cyclic voltammetric analysis to investigate the electrochemical properties of the copolymers, using polymer-coated ITO glass as working electrode supported in 0.1 M $(n\text{-Bu})_4NClO_4$ in acetonitrile. Fig. 7 depicts the cyclic voltammograms of **P1** and **P2** films and Table 3 summarizes the electrochemical data of **PFO** and **P1**–**P3** films. The onset

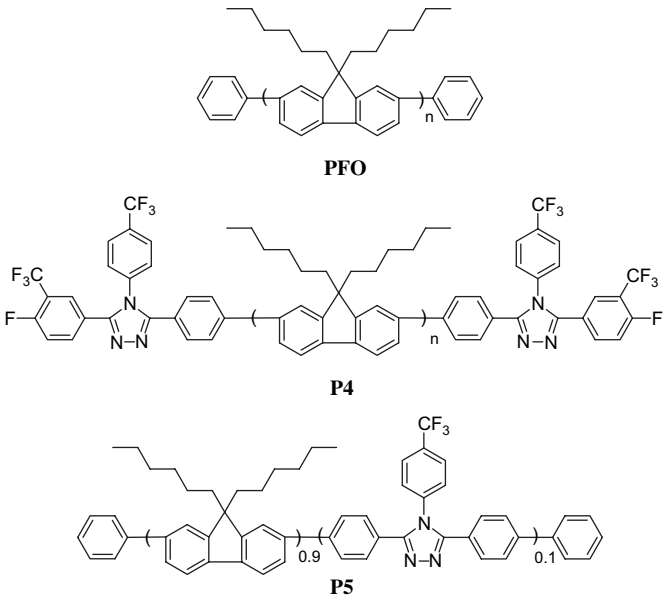

Scheme 2.

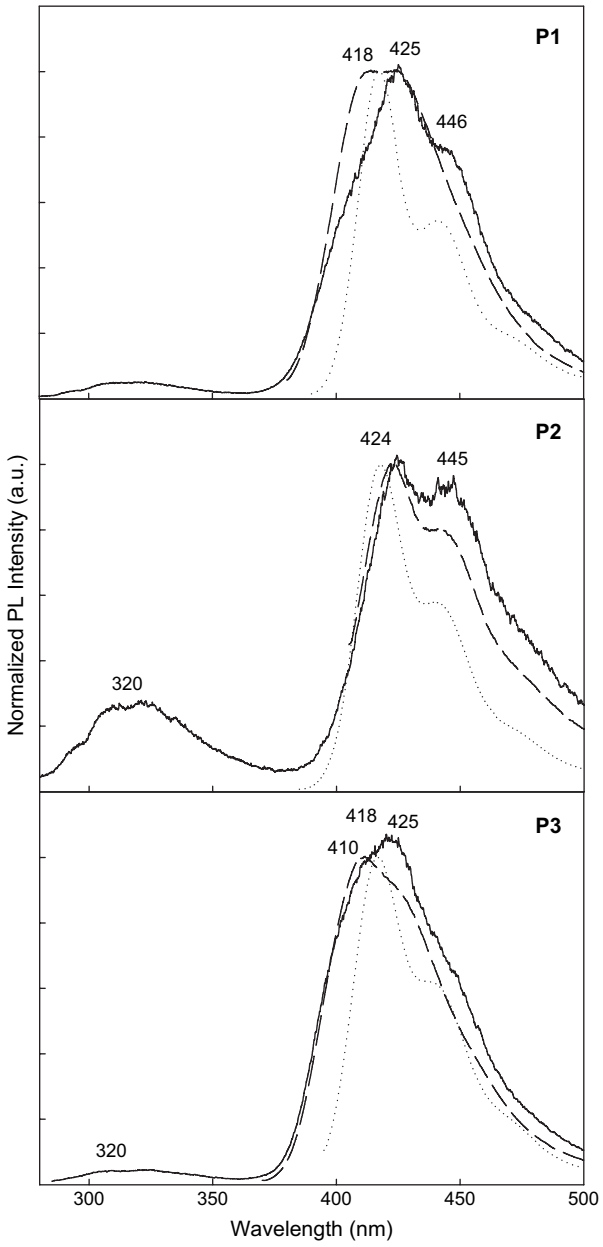

Fig. 6. PL spectra of **P1**–**P3** in CH_3COOH [(—) excited at 266, and (—) 384 nm], and in $CHCl_3$ [(···) excited at 384 nm].

oxidation and reduction potentials versus ferrocene (FOC) of **PFO** are observed at 0.81 and −2.28 V, respectively. The onset oxidation potentials of **P1**–**P3** are 0.85, 0.82, and 0.82 V, respectively, whereas the onset reduction potentials are −2.00, −1.98, and −2.05 V. Evidently, incorporating aromatic triazole segments into polyfluorene reduces the onset reduction potential, but exerts little effect on onset oxidation potential.

In our previous electrochemical studies about copoly(aryl ether)s containing isolated alternate hole- and electron-transporting segments, we had verified that the oxidation and reduction started at the former and the latter segments, respectively, and electron and hole affinities could be enhanced simultaneously [22,30]. Furthermore, this characteristic was also observed in poly(*p*-phenylene vinylene) derivatives containing triazole or oxadiazole segments which have twisted

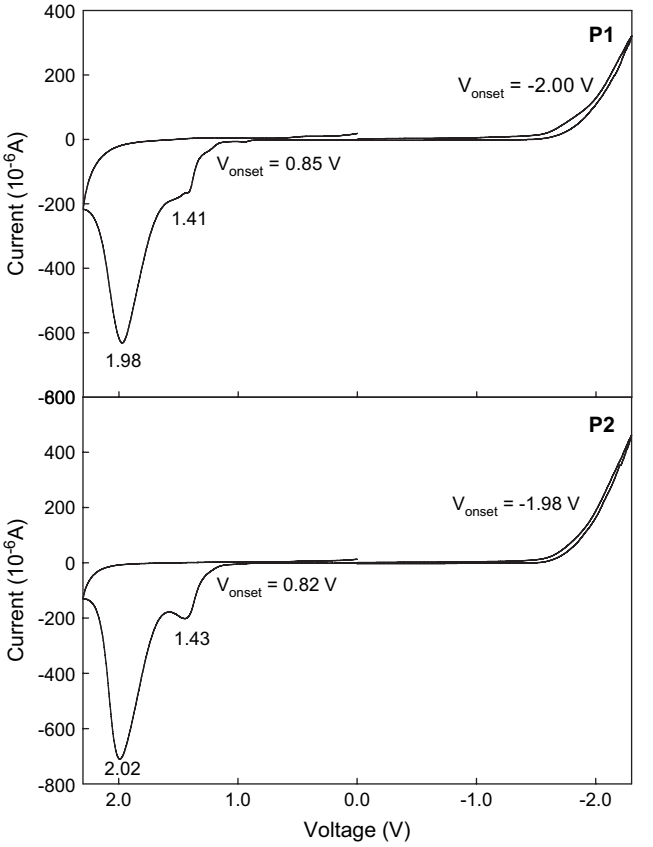

Fig. 7. Cyclic Voltammograms of **P1** and **P2** films coated on ITO glass (scan rate: 100 mV/s).

architecture between hole- and electron-transporting segments [15,16]. Similar phenomena have also been observed in **P1**–**P3** with twisted structure between oligofluorene and triazole segments. And accordingly it is reasonable to suggest that oxidation and reduction proceed from oligofluorene and triazole segments, respectively.

The highest occupied molecular orbital (HOMO), lowest unoccupied molecular orbital (LUMO) levels and band gaps (E_g^{el}) of **P1**–**P3** can be readily calculated from their electrochemical data (Table 3). The HOMO and LUMO energy levels of **P1**–**P3** are −5.65, −5.62, −5.62 eV and −2.80, −2.82, −2.75 eV, respectively. The LUMO levels decrease slightly

Table 3
Electrochemical data of **P1**–**P5**

No.	$E_{onset(red)}$ (V) vs. FOC	$E_{onset(ox)}$ (V) vs. FOC	E_{LUMO} [a] (eV)	E_{HOMO} [b] (eV)	E_g^{el} [c] (eV)	E_g^{opt} [d] (eV)
PFO	−2.28	0.81	−2.52	−5.61	3.09	2.91
P1	−2.00	0.85	−2.80	−5.65	2.85	2.88
P2	−1.98	0.82	−2.82	−5.62	2.80	2.90
P3	−2.05	0.82	−2.75	−5.62	2.87	2.94
P4[e]	−2.13	0.82	−2.67	−5.61	2.91	2.89
P5[e]	−2.09	0.83	−2.71	−5.62	2.91	2.88

[a] $E_{LUMO} = -(E_{onset(red),FOC} + 4.8\ V)eV$.
[b] $E_{HOMO} = -(E_{onset(ox),FOC} + 4.8\ V)eV$.
[c] Band gaps are obtained from electrochemical data.
[d] Band gaps are obtained from onset absorption ($E_g = hc/\lambda_{onset}$).
[e] The data are cited from Ref. [25].

from −2.52 eV of **PFO** to −2.82 eV of **P2** with increasing aromatic triazole contents, confirming that aromatic triazole is an effective chromophore in enhancing electron affinity.

4. Conclusion

We have successfully synthesized and characterized three novel poly(9,9-dihexylfluorene) derivatives **P1**–**P3** containing aromatic triazole chromophores whose functionality and linkage are different. They are readily soluble in common organic solvents such as THF, chloroform and 1,1,2,2-tetrachloroethane. Thermal decomposition temperatures (T_ds) of **P1**–**P3** are between 416 and 454 °C. The optical and electrochemical properties of **P1**–**P3** were compared with those of poly(9,9-dihexylfluorene) (**PFO**) and **P4** and **P5**. Both absorption and PL emission peaks of **P1**–**P3** show blue shift after introducing the aromatic triazole units due to confined main-chain conjugation. Moreover, incorporation of aromatic triazole segments in **P1**–**P3** increases their PL efficiencies. The HOMO and LUMO energy levels of **P1**–**P3** are −5.65, −5.62, −5.62 eV and −2.80, −2.82, −2.75 eV, respectively, while those of **PFO** are −5.61 and −2.52 eV. Present results suggest that aromatic triazoles partially inhibit excimer formation and enhance electron affinity of **PFO**.

References

[1] Burroughes JH, Bradley DDC, Brown AR, Marks RN, Mackay K, Friend RH, et al. Nature 1990;347:539.
[2] Gustafsson G, Cao Y, Treacy GM, Klavetter F, Colaneri N, Heeger AJ. Nature 1992;357:477.
[3] Akcelrud L. Prog Polym Sci 2003;28:875.
[4] Liao L, Pang Y, Ding L, Karasz FE. Macromolecules 2002;35:3819.
[5] Shu CF, Dodda R, Wu FI, Liu MS, Jen AKJ. Macromolecules 2003; 36:6698.
[6] Mikroyannidis JA, Spiliopoulos IK, Kasimis TS, Kulkarni AP, Jenekhe SA. Macromolecules 2003;36:9295.
[7] Kraft A, Grimsdale AC, Holmes AB. Angew Chem Int Ed Engl 1998; 37:402.
[8] Liu CH, Chen SH, Chen Y. J Polym Sci Part A Polym Chem 2006;44: 3882.
[9] Hwang SW, Chen Y, Chen SH. J Polym Sci Part B Polym Phys 2003; 42:333.
[10] Menon A, Dong H, Niazimbetova ZI, Rothberg LJ, Galvin ME. Chem Mater 2002;14:3668.
[11] Burn PL, Holmes AB, Kraft A, Bradley DDC, Brown AR, Friend RH, et al. Nature 1992;356:47.
[12] Hwang SW, Chen Y. Polymer 2000;41:6581.
[13] Hwang SW, Chen Y. Macromolecules 2002;35:5438.
[14] Zheng S, Shi J, Mateu R. Chem Mater 2000;12:1814.
[15] Chen SH, Chen Y. Macromolecules 2005;38:53.
[16] Chen SH, Chen Y. J Polym Sci Part A Polym Chem 2006;44:4514.
[17] Chen SH, Chen Y. Macromol Chem Phys 2006;207:1070.
[18] Knupfer M, Fink J, Zojer E, Leising G, Scherf U, Mullen K, et al. Macromolecules 1999;32:361.
[19] Jin SH, Kang SY, Kim MY, Chan YU, Kim JY, Lee K, et al. Macromolecules 2003;36:3841.
[20] Hwang SW, Chen SH, Chen Y. J Polym Sci Part A Polym Chem 2002; 40:2215.
[21] Kreyenschimdt M, Klaerner G, Fuhrer T, Ashenhurst J, Karg S, Chen W, et al. Macromolecules 1998;31:1099.
[22] Chen SH, Chen Y. J Polym Sci Part A Polym Chem 2004;42:5900.
[23] Grice AW, Tajbakhsh A, Burn PL, Bradley DDC. Adv Mater 1997; 9(15):1174.
[24] Strukelj M, Papadimitrakopoulos F, Miller TM, Rothberg LJ, Chandross EA. Science 1995;117:11976.
[25] Chen SH, Chen Y, Shiau CS, Tsai CJ. J Polym Sci Part A Polym Chem, in press.
[26] Liu Y, Liu MS, Jen AKY. Acta Polym 1999;50:105.
[27] MNDO semi-empirical calculations and molecular orbitals were performed with Gaussian R 98W and Gauss View 3.09 by Gaussian, Inc.
[28] Bliznyuk VN, Carter SA, Scott JC, Klarner G, Miller RD, Miller DC. Macromolecules 1999;32:361.
[29] Liu L, Tang S, Liu M, Xie Z, Zhang W, Lu P, et al. J Phys Chem B 2006;110:13734.
[30] Chen SH, Chen Y. J Polym Sci Part A Polym Chem 2005;43:5083.
[31] Monkman AP, Palsson LO, Higgins RWT, Wang C, Bryce MR, Batsanov AS, et al. J Am Chem Soc 2002;124:6049.